Supporting information for:

Enhanced Luminescence and Mechanistic Studies on Layered Double Perovskite Phosphors: $Cs_4Cd_{1-x}Mn_xBi_2Cl_{12}$

Brenda Vargas,[†] Diana T. Reyes-Castillo,[†] Eduardo Coutino-Gonzalez,[⊥] Citlali Sánchez-Aké,[œ] Carlos Ramos,[†] Ciro Falcony,[‡] and Diego Solis-Ibarra*[†]

[†] Instituto de Investigaciones en Materiales, Universidad Nacional Autónoma de México, CU, Coyoacán, 04510, Ciudad de México, México

[⊥] Centro de Investigaciones en Óptica, A. C., Loma del Bosque 115, Colonia Lomas del Campestre, León, Guanajuato, 37150, Mexico

[œ] Instituto de Ciencias Aplicadas y Tecnología, Universidad Nacional Autónoma de México, CU, Coyoacán, 04510, Ciudad de México, México

[‡] Departamento de Física, Centro de Investigación y de Estudios Avanzados del IPN, Instituto Politécnico Nacional 2508, San Pedro Zacatenco, Gustavo A. Madero Cuidad de México, 07360, México

*E-mail: diego.solis@unam.com

π

Table S1. Amounts of cadmium and manganese precursors used for the synthesis of $Cs_4Cd_{1-x}Mn_xBi_2Cl_{12}$.

Mn content x	$CdCl_2$ mass (mg)	$MnCl_2$ mass (mg)
0.0	91.6	0
0.15	77.9	9.6
0.2	73.3	12.8
0.3	64.1	19.5
0.5	45.8	32.1
1.0	0	65

Table S2. Amounts of cadmium and manganese precursors added during synthesis of $Cs_4Cd_{1-x}Mn_xBi_2Cl_{12}$ for lower Mn concentrations.

Mn content x	$CdCl_2$ mass (mg)	$MnCl_2$ mass (mg)
0.05	174.2	6.4
0.10	165	12.8

Figure S1. Comparison between PXRD diffractograms of the $Cs_4Cd_{1-x}Mn_xBi_2Cl_{12}$ family of <111>-oriented layered perovskites with increasing Mn content (x) and theoretical diffractograms obtained from the Rietveld refinement of the $Cs_4CdBi_2Cl_{12}$ and $Cs_4MnBi_2Cl_{12}$ materials (black lines).[1]

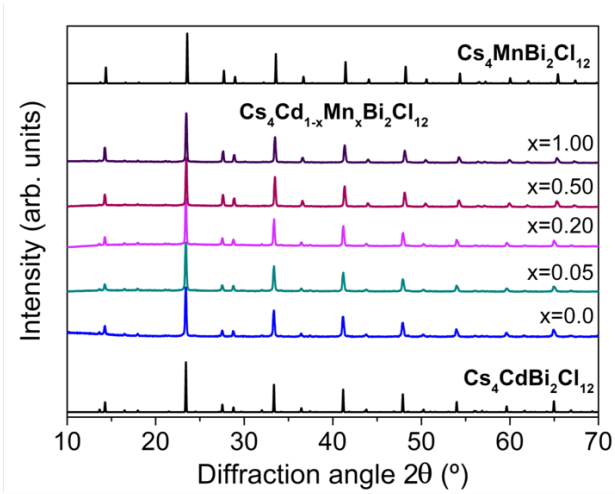

Figure S2. Thermogravimetric analysis of A) $x = 0.0$, B) $x = 0.05$, C) $x = 0.10$, D) $x = 0.20$ and, E) $x = 1.0$.

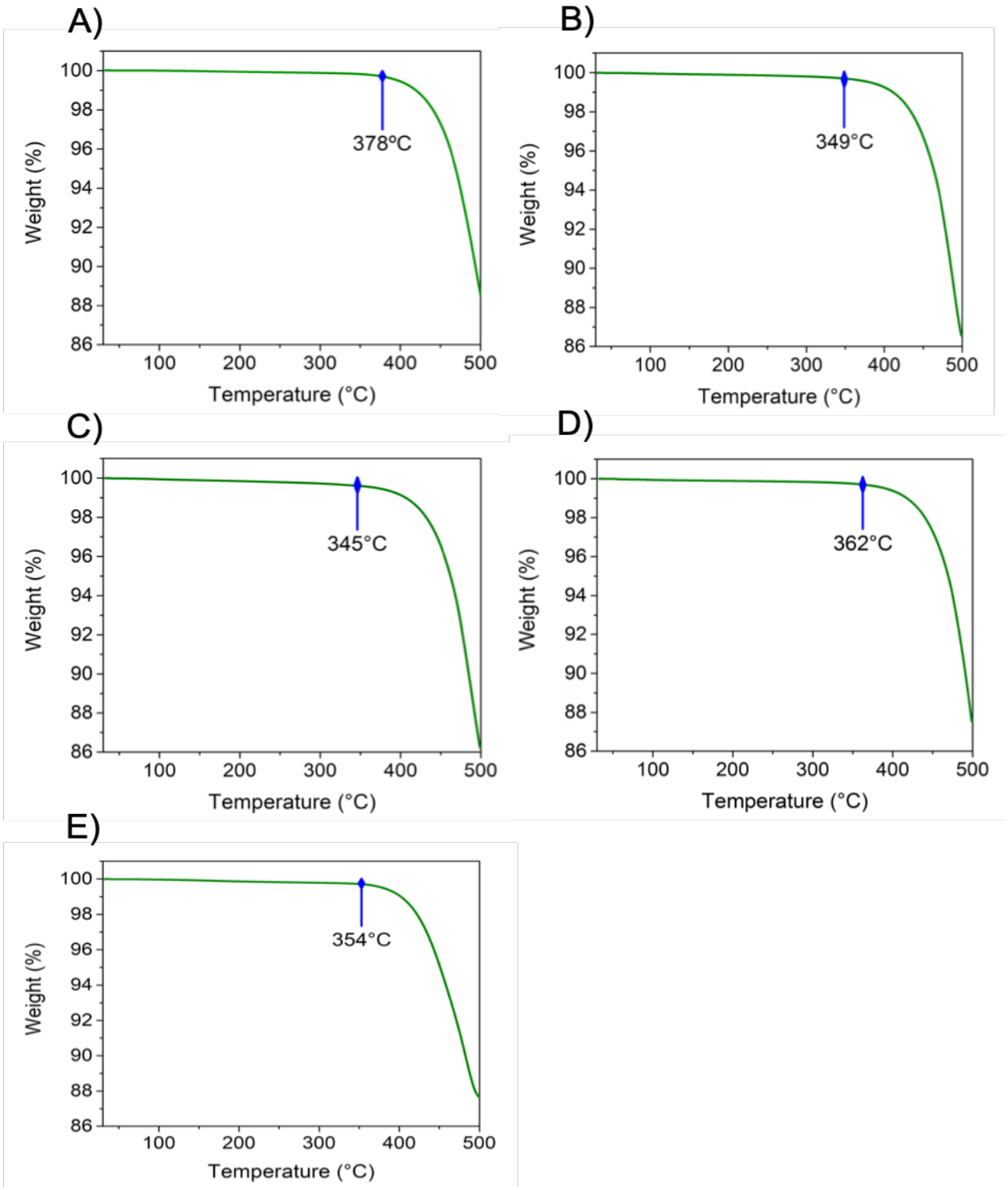

Figure S3. Differential scanning calorimetry of A) $Cs_4CdBi_2Cl_{12}$ and B) $Cs_4MnBi_2Cl_{12}$.[1]

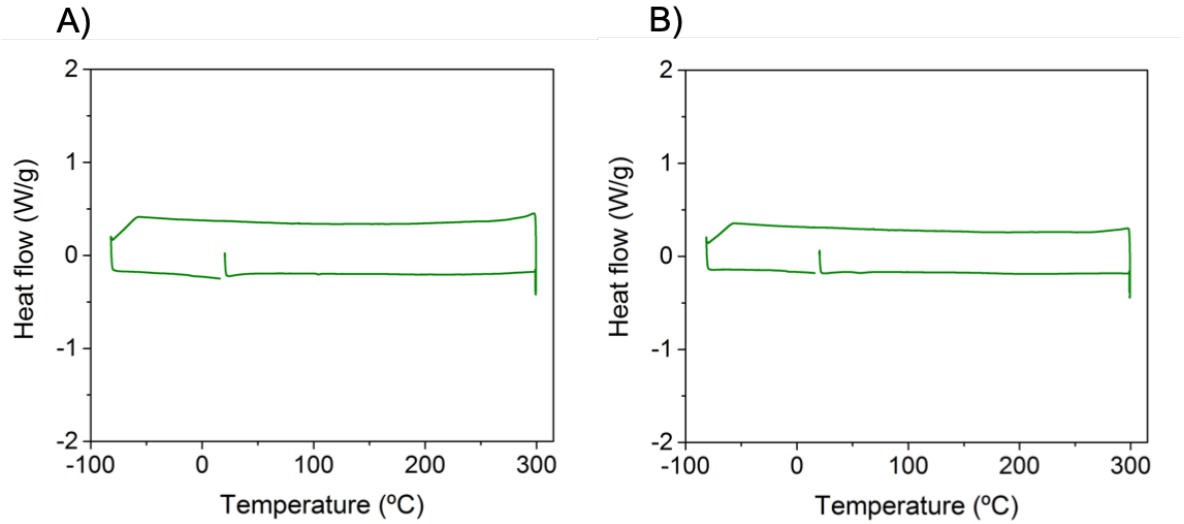

Figure S4. Normalized absorbance spectra calculated from diffuse reflectance measurements of the materials for x = 0.0, 0.05, 0.10, 0.15, 0.20, 0.30, 0.50 and 1.0.

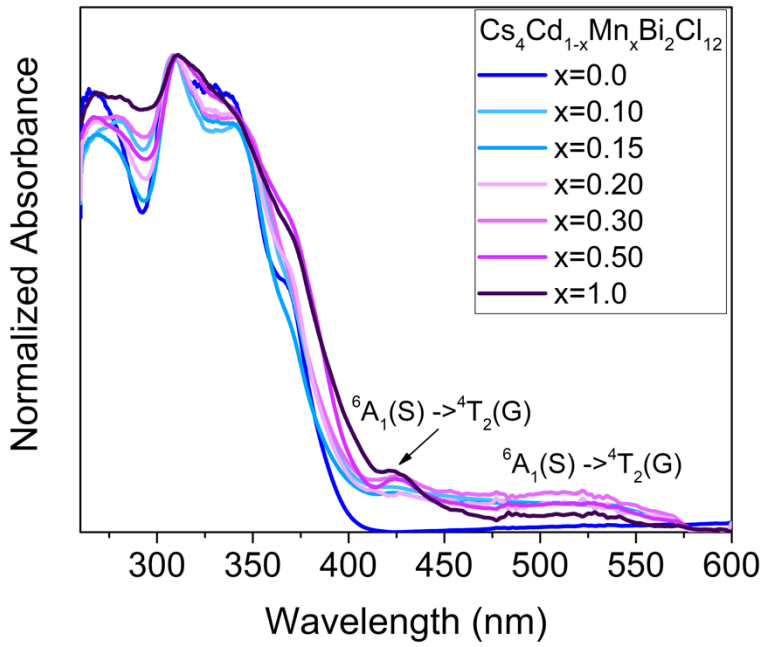

Table S3. Direct and indirect band gaps of the Mn-containing materials obtained from Tauc plots.

Mn content	Direct (eV)	Indirect (eV)
0.0	3.17	2.91
0.05	3.12	2.89
0.10	3.10	2.87
0.20	3.12	2.87
0.30	3.11	2.85
0.50	3.14	2.88
1.0	3.11	2.71

Figure S5. A) Excitation spectra at different emission wavelengths and B) emission spectra obtained at different excitation wavelengths for the material with x = 0.20.

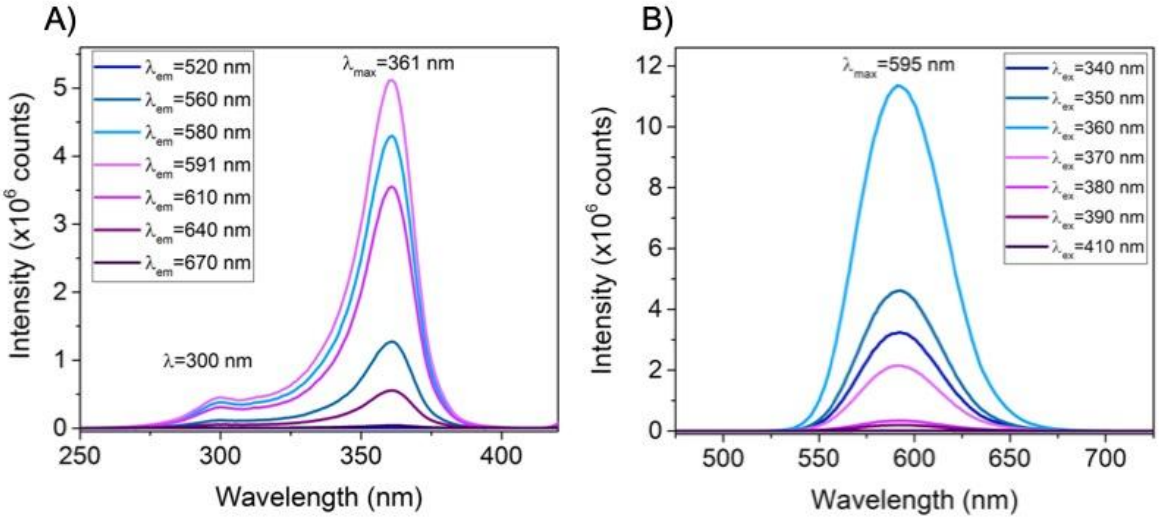

Figure S6. Emission and excitation 3D plots for x = A) 0.05, B) 0.10, C) 0.20, D) 0.30, E) 0.50 and F) 1.0.

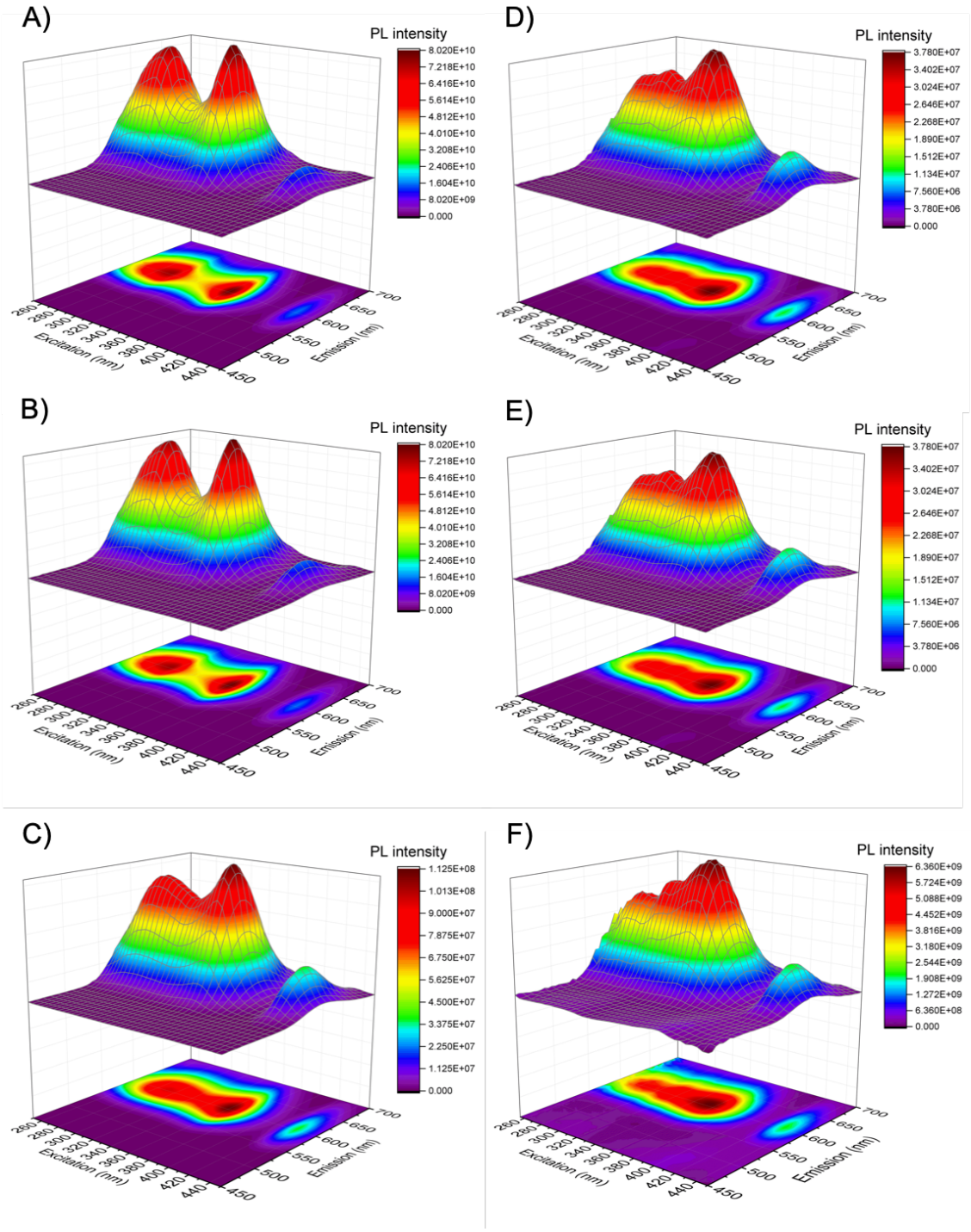

Figure S7. Absorbance (dark blue), excitation (light blue) and emission (pink) spectra for samples with Mn content x = 0.0, 0.05, 0.10, 0.20, 0.5 and 1.0.

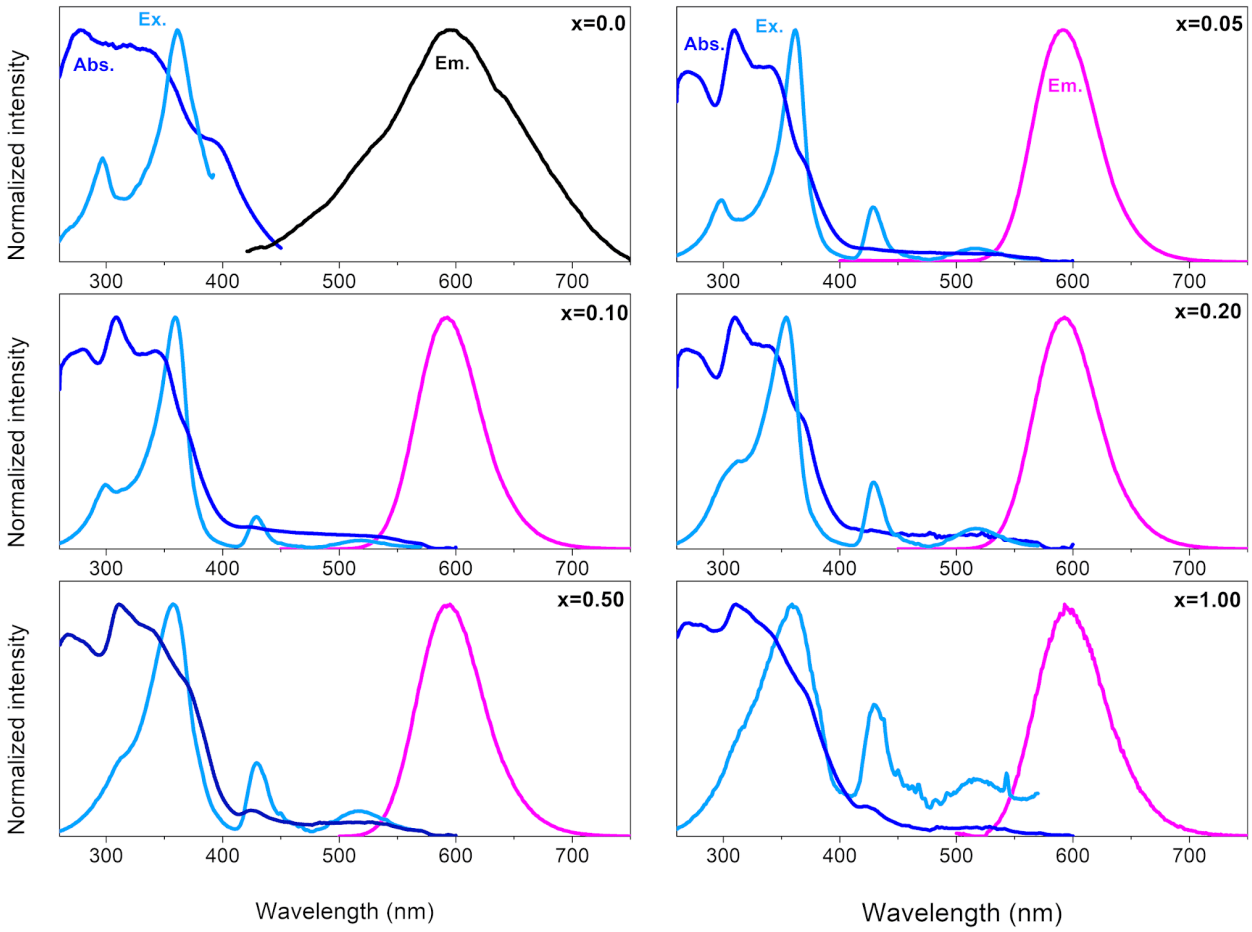

Figure S8. A) Normalized excitation and emission spectra for Mn content of x = 0.05, 0.10, 0.15, 0.20, 0.50 and 1.00, and B) inset of peak emission to show the red shift with increasing Mn content.

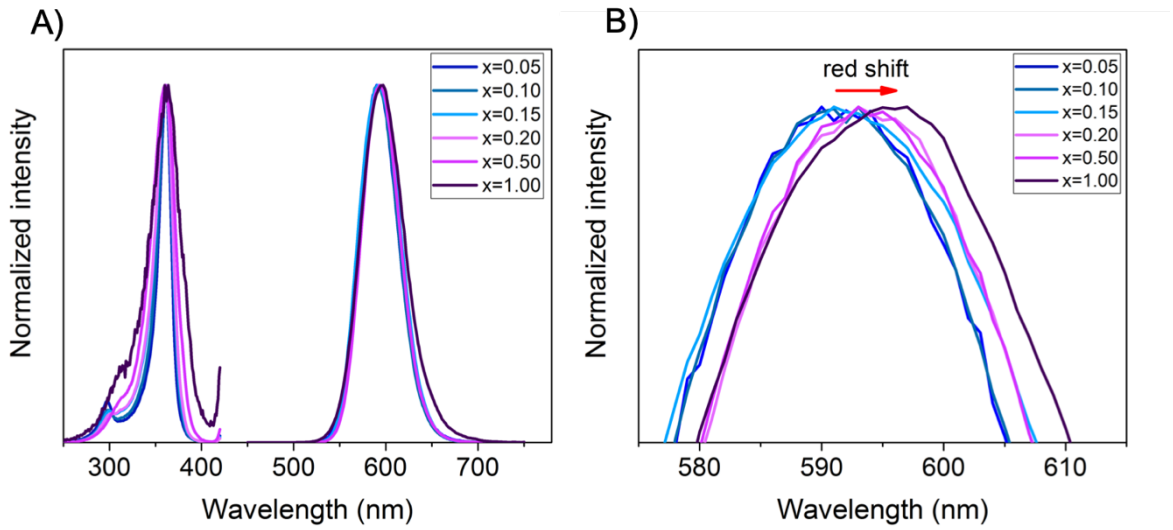

Figure S9. Distance between Mn^{2+} first next neighbors in $Cs_4MnBi_2Cl_{12}$.

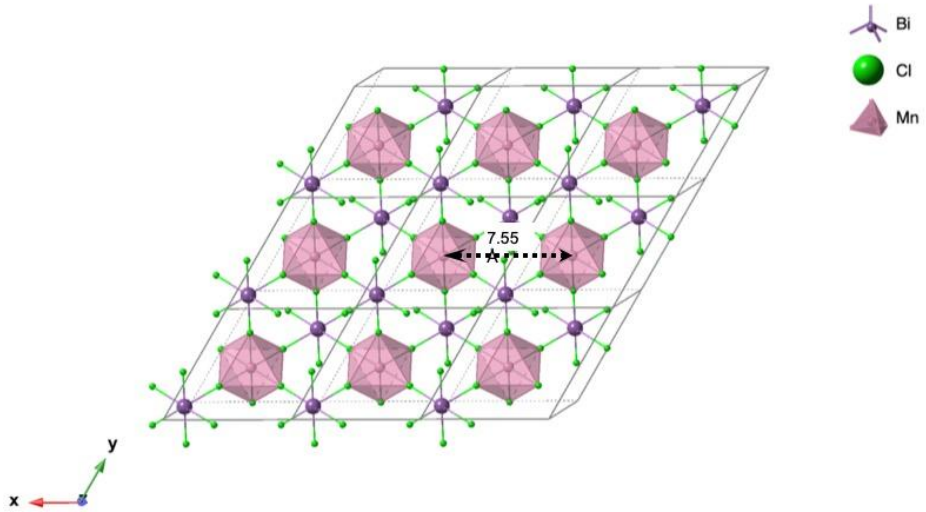

Figure S10. Schematic representation of the fluorometer and the integrating sphere used in this study. The configuration "in" and "out" of the beam are indicated on the left side of the diagram.

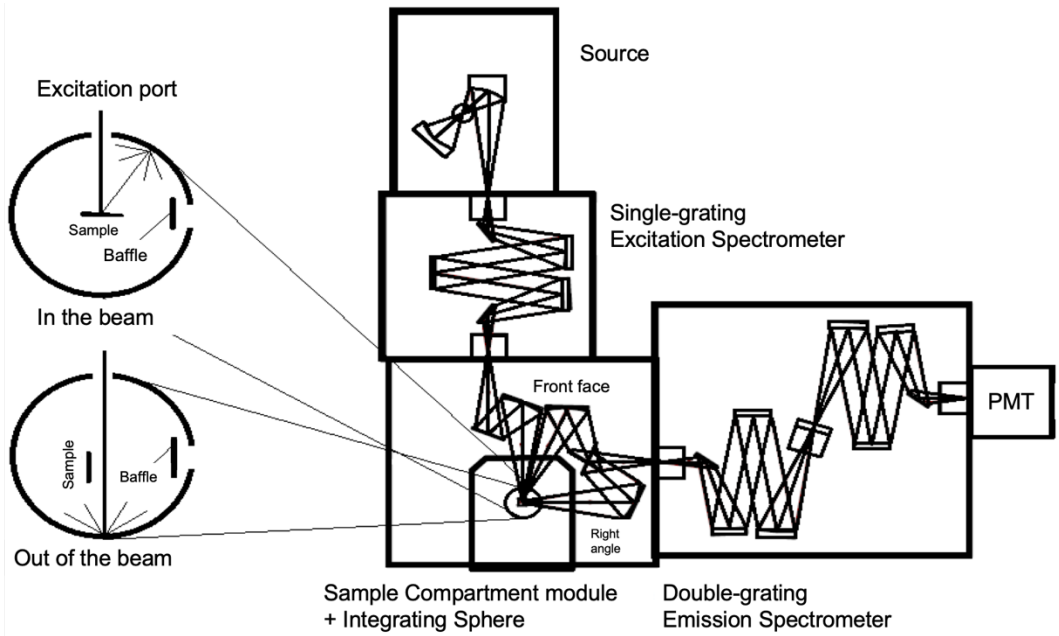

Note on external quantum efficiency

Next to price, the major decisive factor for such application is the external quantum efficiency (EQE). The EQE of a luminescent material is defined as the ratio of the number of photons emitted to the number of incident photons, this measure takes into account losses associated with the absorption of photons by non-emissive species.[2] PLQY measurements are at most equal to EQE but are in general lower.

Figure S11. Integrated PL intensity vs temperature (black line) and the adjustment according equation (S1) in red, for materials with A) $x = 0.05$ and B) $x = 0.20$.

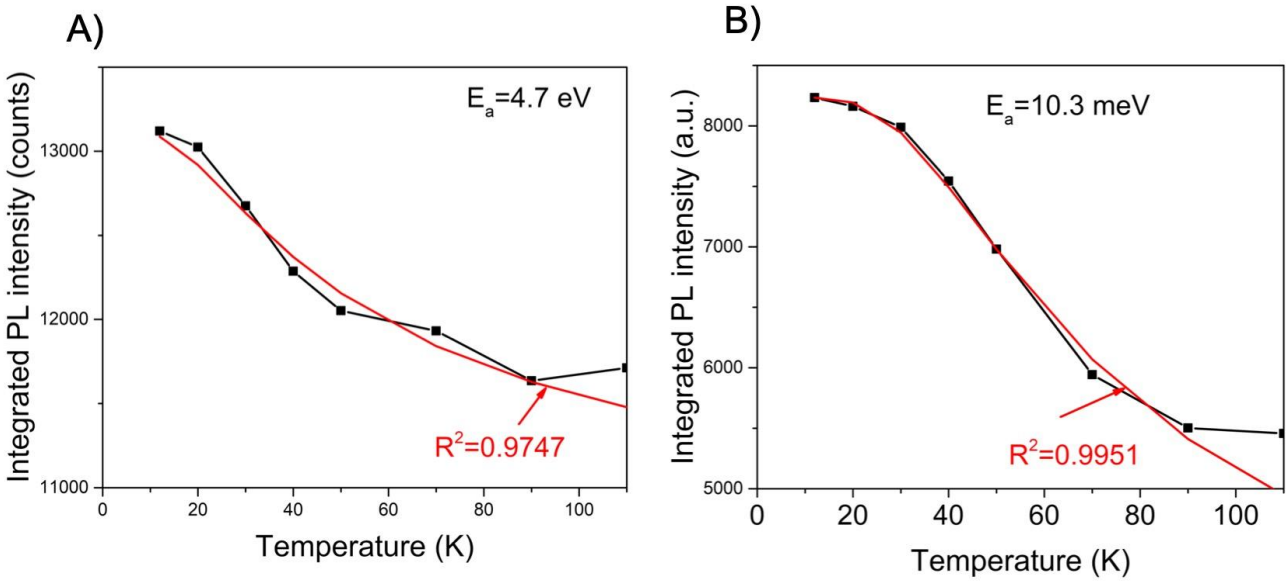

Fitting of the Temperature-dependent PL measurements

Based on the theory of thermal quenching, the temperature dependence of the emission intensity, I(T), can be described by

$$I(T) = I_0 / 1 + A\exp(-E_a/kT) \qquad \textbf{(S1)}$$

where E_a is the activation energy (thermal quenching energy), k is the Boltzmann constant, a is a constant related to the ratio of the nonradiative rate to the radiative rate, and I_0 is the emission intensity at 0 K. The red solid lines in Figure S11 represent a simulation of the intensities using equation S1.[3]

Fitting of the Time-resolved PL measurements

The decay profiles for Mn content between x = 0.05 and 0.20 can be fitted using a biexponential function:

$$I(T) = A_1 \exp(-t / \tau_1) + A_2 \exp(-t / \tau_2) \qquad \textbf{(S2)}$$

The decay profiles for Mn content with x = 0.05 and 1.0 can be fitted with a triexponential function:

$$I(T) = A_1 \exp(-t / \tau_1) + A_2 \exp(-t / {}_2) + A_3 \exp(-t / \tau_3) \qquad \textbf{(S3)}$$

Table S4. Amplitude and lifetimes of the materials with increasing Mn content.

Mn content	A_1	τ_1 (μs)	A_2	τ_2 (μs)	A_3	τ_3 (μs)
0.05	0.00238	45.8	0.00608	396.6		
0.10	0.00293	41.5	0.00644	374.3		
0.15	0.00339	37.7	0.00583	363.8		
0.20	0.0039	36.3	0.00641	359.2		
0.50	0.00338	11.1	0.00177	127.5	127.5	1.2
1.00	0.00466	2.1	0.00155	11.7	0.01036	0.4

Figure S12. Decay lifetimes τ_1 (black line) and τ_2 (red line) from Mn^{2+} pairs and isolated Mn^{2+}, respectively.

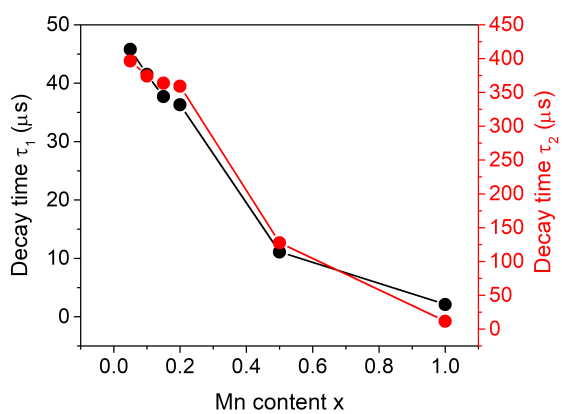

.

References

[1] B. Vargas, R. Torres-Cadena, D. T. Reyes-Castillo, J. Rodríguez-Hernández, M. Gembicky, E. Menéndez-Proupin, D. Solis-Ibarra, *Chem. Mater.* **2020**, *32*, 424–429.

[2] S. Leyre, E. Coutiño-Gonzalez, J. Joos, J. Ryckaert, Y. Meuret, D. Poelman, G. Durinck, J. Hofkens, G. Deconinck, P Hanselaer, *Rev. Sci. Instrum*. **2014**, *85*, 123115(1-9).

[3] C. Wei, A. G. Joly, J.-O. Malm, J.-O. Bovin, S. Wang, J. Phys. Chem. B **2003**, 107, 6544-6551.